

CT imaging with truncated data over limited-angular ranges

Dan Xia^a, Zheng Zhang^a, Buxin Chen^a, Emil Y. Sidky^a, and Xiaochuan Pan^{a,b}

^aDepartment of Radiology, The University of Chicago, Chicago, IL, USA

^bDepartment of Radiation & Cellular Oncology, The University of Chicago, Chicago, IL, USA

ABSTRACT

In certain CT applications such as dental CT imaging, a scanning configuration with an offset-detector is often used for extending the field of view (FOV) of the system. While data are truncated on one-side of the detector, it remains possible to accurately reconstruct an image from the truncated data collected over a full-angular range (FAR) of 360° by use of existing analytical-based algorithms such as the FDK algorithm. However, there also exist interests in scanning configurations that collect data only over limited-angular ranges (LARs) for practical considerations, and existing algorithms generally yield reconstructions with significant artifacts from LAR data collected with an offset-detector. It has been demonstrated recently that, for non-truncated data, the directional-total-variation (DTV) algorithm can reconstruct images with significantly reduced artifacts from LAR data. In this work, we developed and tailored the DTV algorithm for image reconstruction from truncated LAR data collected with a scanning configuration employing an offset-detector. We carried out a study on image reconstruction for a number of LAR scanning configurations with an offset-detector of practical interest. The study results demonstrate that the DTV algorithm can be tailored to yield, from truncated LAR data, images with significantly reduced artifacts that are observed otherwise in images obtained with existing analytical-based algorithms.

1. INTRODUCTION

In certain CT applications, a scanning configuration with an offset-detector is used often for effectively increasing its field of view (FOV).^{1,2} While data collected with an offset-detector at each view are truncated on one side of the detector, accurate images can be reconstructed from the truncated data collected over a full-angular range (FAR) of 360° . It is also recognized that a reduced scanning angular range can be exploited for potentially lowering radiation dose and scanning time and for avoidance of the collisions between the gantry and scanned objects, e.g., in C-arm cone-beam CT (CBCT). Therefore, it is of interest and potential value to investigate scanning configurations with offset-detectors for data collection over limited-angular ranges (LARs) that are considerably shorter than the FAR of 360° . Clearly, existing algorithms, such as the FDK algorithm and its variations widely used for image reconstruction from FAR data collected with an offset-detector, will yield images with significant artifacts when applied to LAR data collected with the same offset-detector.

It has been shown recently that the directional-total-variation (DTV) algorithm can accurately reconstruct images from LAR data without any truncation.^{3,4} In this work, we developed and tailored the DTV algorithm for image reconstruction from truncated LAR data collected with scanning configurations in which an offset-detector is employed. The study results demonstrate that the DTV algorithm can be tailored to yield, from truncated LAR data, images with significantly reduced artifacts that are observed otherwise in images obtained with existing analytical algorithms.

2. MATERIAL AND METHODS

2.1 LAR scanning configuration with an offset-detector

In the work, the X-ray transform⁵ in a discrete form is used as the imaging model, and image reconstruction is equivalent to inverting the imaging model. Clearly, the ill-conditionedness of the imaging model depends upon the LAR extent and distribution over which knowledge of the discrete X-ray transform (DXT), i.e., the imaging model, is available. Without loss of generality, we consider a circular fan-beam configuration with an offset-detector, as shown in Fig. 1a. From the head image in Fig. 1b, truncated data generated with the configuration over an FAR of 360° are shown in Fig. 1c. On the other hand, an LAR scanning configuration with

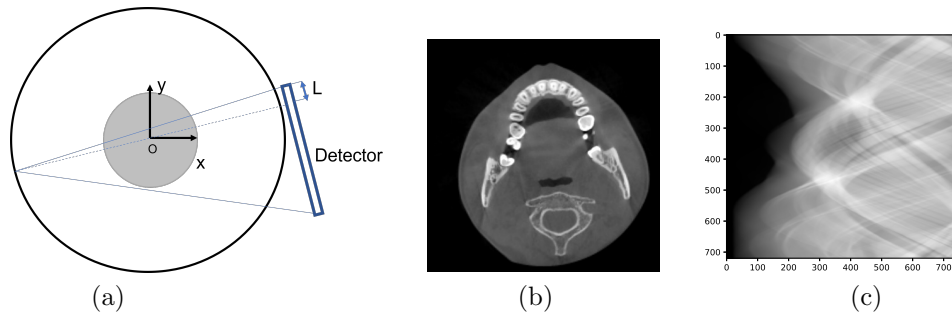


Figure 1. (a) A circular fan-beam scanning configuration with an offset-detector in which O and L denote the rotation center and the length of the detector-offset. (b) The numerical head phantom, and (c) data collected over an FAR of 360° . It can be observed that the data are truncated in the right-hand side of the data space in (c). Display windows are $[0.15, 0.3] \text{ cm}^{-1}$ and $[0, 3]$, respectively.

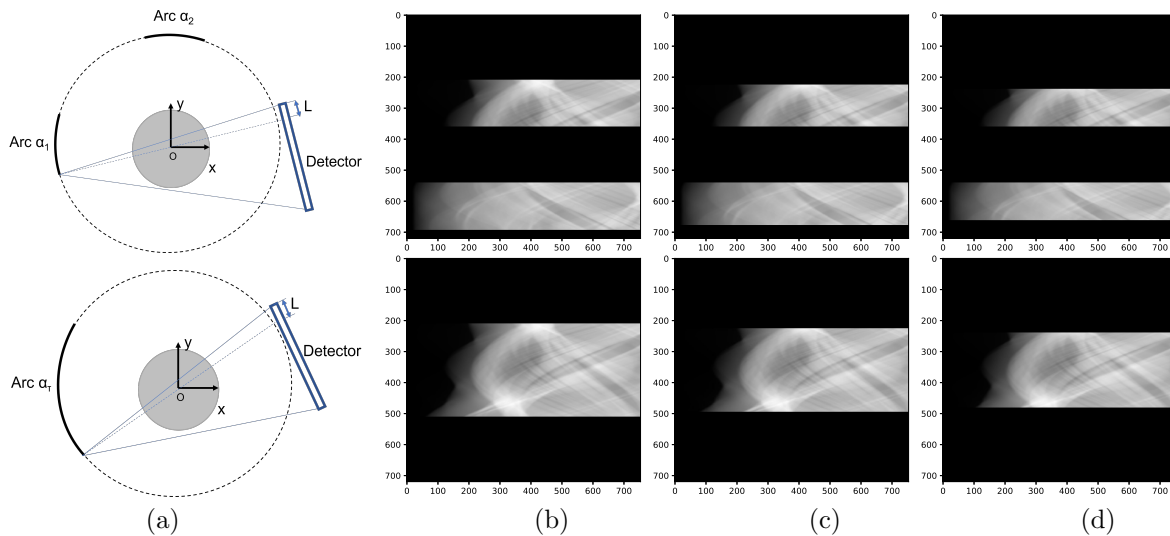


Figure 2. (a) Two-orthogonal-arc (row 1) and single-arc (row 2) scanning configurations with an offset-detector. Data generated with the two-orthogonal-arc scanning configurations (row 1) over LARs $(\alpha_1, \alpha_2) = (75^\circ, 75^\circ)$ (b), $(67.5^\circ, 67.5^\circ)$ (c), and $(60^\circ, 60^\circ)$ (d), and with the single-arc scanning configurations (row 2) over LARs $\alpha_r = 150^\circ$ (e), 135° (f), and 120° (g). Display window is $[0, 3]$.

an offset-detector is shown in row 1 of Fig. 2a, which consists of two orthogonal arc components, separated by 90° , indicated by arcs α_1 and α_2 , where α_1 and α_2 indicate their angular ranges. We refer to this configuration as a two-orthogonal-arc (TOA) LAR configuration, and thus as a single-arc (SA) LAR configuration if $\alpha_1 = 0$ or $\alpha_2 = 0$ as displayed in row 2 of Fig. 2a. We investigated image reconstruction from data, as shown in Figs. 2b-2d, collected over the TOA and SA scanning configurations, of the same total angular range, with an offset-detector.

In the circular fan-beam configuration, the distances from the X-ray source to the detector and to the rotation center are 60 and 40 cm, respectively. The detector consists of 754 elements with a size of 0.2 mm. A detector-offset $L = 30$ mm is used for yielding an extended FOV. The head phantom shown in Fig. 1b consists of 200×200 pixels of size 0.8×0.8 mm².

Using the head phantom, we first generate data, as shown in Fig. 1c over an FAR of 360° with an angular interval of 0.5° per view. For each view, the generated data are truncated on one side of the detector as a result of the detector-offset. We consider TOA scanning configurations with LARs $(\alpha_1, \alpha_2) = (75^\circ, 75^\circ)$, $(67.5^\circ, 67.5^\circ)$, and $(60^\circ, 60^\circ)$, and use them to generate data from the head phantom, as shown in row 1 of Figs. 2b-2d. For comparison, we have also investigated image reconstruction from data of the head phantom generated over SAs with LARs $\alpha_\tau = \alpha_1 + \alpha_2 = 150^\circ, 135^\circ, 120^\circ$, as shown in row 2 of Figs. 2b-2d.

In addition, using noiseless LAR data generated above, we created noisy LAR data by adding the Poisson noise, corresponding to 10^7 noise equivalent quanta (NEQ) per detector bin in air scans, and we subsequently performed image reconstructions from the noisy LAR data.

2.2 Image reconstruction

For CT scans over TOA or SA LAR with an offset-detector, the image reconstruction can be formulated as the solution to a constrained optimization program in which a weighted data- ℓ_2 fidelity is minimized under image-DTV constraints along the x - and y -directions. The optimization program is given by

$$\mathbf{f}^* = \underset{\mathbf{f}}{\operatorname{argmin}} \left\{ \frac{1}{2} \| W(\mathcal{H}\mathbf{f} - \mathbf{g}^{[M]}) \|_2^2 \right\}$$

$$\text{s.t. } \| \mathcal{D}_x \mathbf{f} \|_1 \leq t_1, \| \mathcal{D}_y \mathbf{f} \|_1 \leq t_2, \text{ and } f_i \geq 0, \quad (1)$$

where vector $\mathbf{g}^{[M]}$ of size M denotes discrete measured data acquired with two-orthogonal-arc or single-arc LAR scanning configuration; vector \mathbf{f} of size N is a 2D discrete image; f_i is the entry i of \mathbf{f} ; \mathcal{H} the system matrix of size $M \times N$ representing the X-ray transform, with element $h_{j,i}$ representing the contribution of pixel i to ray j ; W is an $M \times M$ diagonal matrix in which each diagonal element represents a positive weighting factor for a corresponding X-ray measurement; $\| \cdot \|_p$ indicates the ℓ_p -norms of the input vector for $p = 1$ and 2 ; matrices \mathcal{D}_x and \mathcal{D}_y of size $N \times N$ denote two-point differences along the x - and y -axes, respectively; vectors $\mathcal{D}_x \mathbf{f}$ and $\mathcal{D}_y \mathbf{f}$ are of size N ; and parameters t_1 and t_2 depict the upper bounds on the DTV constraints along x - and y -directions.

Weighting matrix W is introduced for controlling the numerical effect of the discontinuity of truncated data on image reconstruction. Different designs of weighting matrix W may result in different reconstruction programs, leading to different reconstructions when data are inconsistent with the imaging model.

Based upon the general primal-dual optimization framework,^{6,7} a DTV algorithm was developed previously for solving the constrained optimization program minimizing data- ℓ_2 fidelity without weighting matrix W under DTV constraints.^{3,4,8,9} In this work, we tailored the DTV algorithm to solve Eq. (1) including a weighting factor W for image reconstruction from truncated data acquired with the offset-detector.

3. RESULTS

3.1 Reconstruction from noiseless data

Using the tailored DTV algorithm, we first reconstruct images of the head phantom from noiseless data generated over a number of TOAs with LARs $(\alpha_1, \alpha_2) = (75^\circ, 75^\circ)$, $(67.5^\circ, 67.5^\circ)$, and $(60^\circ, 60^\circ)$, (i.e., data in row 1 of Figs. 2b-2d), and display the reconstructed images in row 1 of Fig. 3. In an attempt to compare the differences

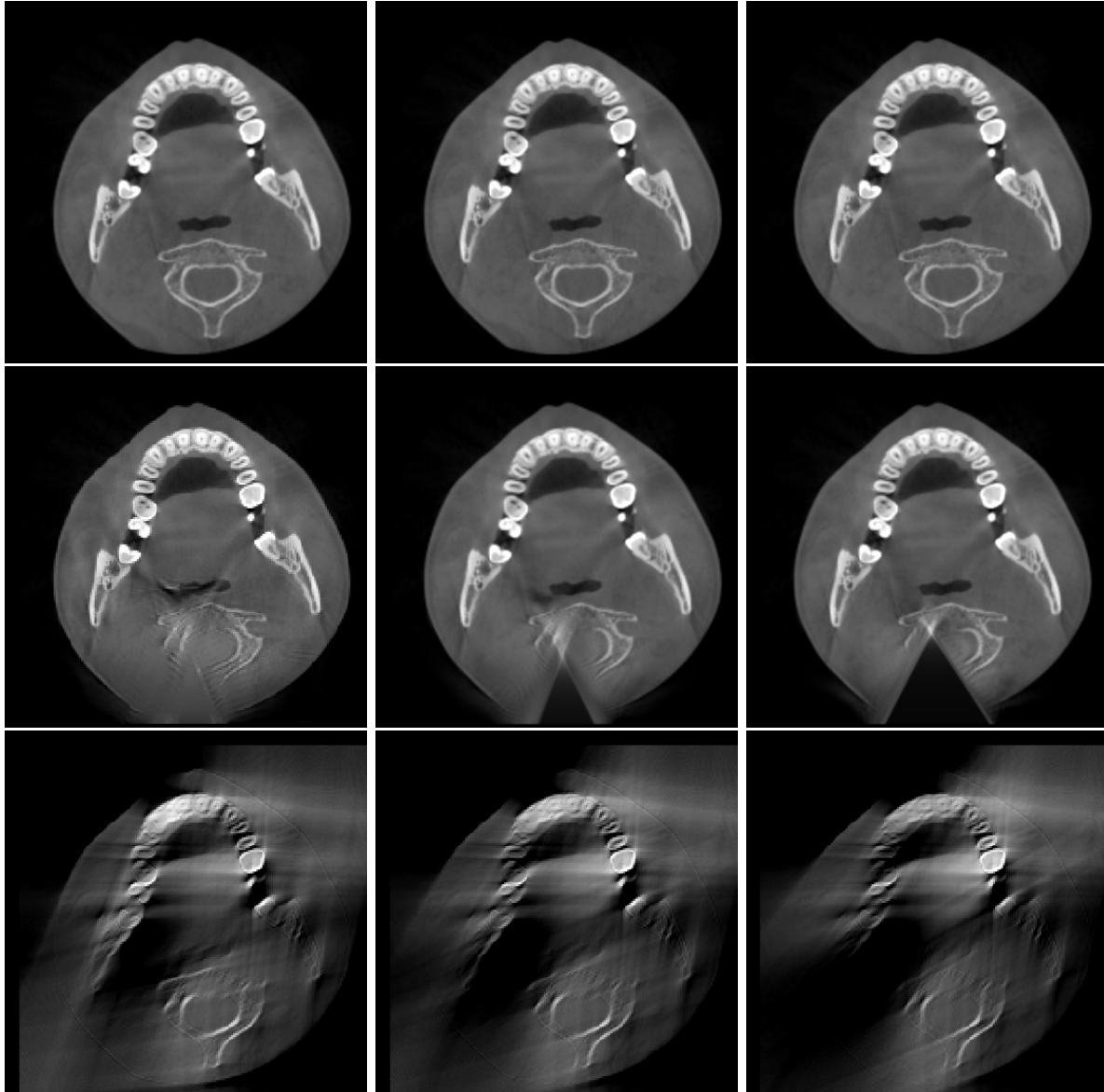


Figure 3. Row 1: images reconstructed by use of the DTV algorithm from noiseless data of TOA scanning configurations over LARs $(\alpha_1, \alpha_2) = (75^\circ, 75^\circ)$ (a), $(67.5^\circ, 67.5^\circ)$ (b), and $(60^\circ, 60^\circ)$ (c); row 2: images reconstructed by use of the DTV algorithm from noiseless data of SA scan configurations over LARs $\alpha_\tau = 150^\circ$ (a), 135° (b), and 120° (c); and row 3: images reconstructed by use of the FDK algorithm from noiseless data of TOA scanning configurations used for obtaining images in row 1. Display window is $[0.0, 0.6] \text{ cm}^{-1}$.

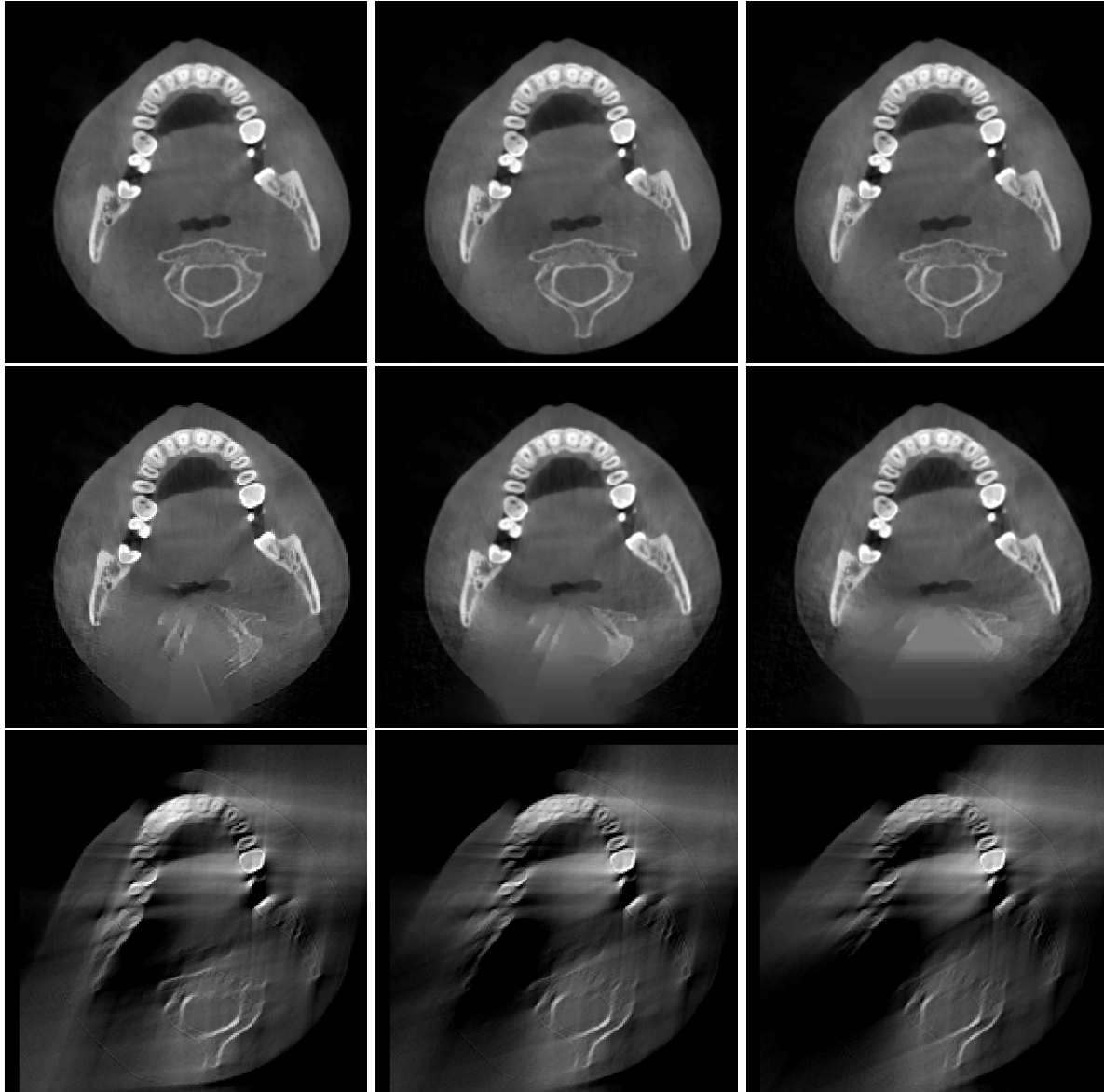


Figure 4. Row 1: images reconstructed by use of the DTV algorithm from noisy data of two-orthogonal-arc scanning configurations over LARs $(\alpha_1, \alpha_2) = (75^\circ, 75^\circ)$ (a), $(67.5^\circ, 67.5^\circ)$ (b), and $(60^\circ, 60^\circ)$ (c); row 2: images reconstructed by use of the DTV algorithm from noisy data of single-arc scanning configurations over LARs $\alpha_\tau = 150^\circ$ (a), 135° (b), and 120° (c); and row 3: images reconstructed by use of the FDK algorithm from noisy data of two-orthogonal-arc scanning configurations used for obtaining images in row 1. Display window is $[0.0, 0.6] \text{ cm}^{-1}$.

between TOA and SA LAR reconstructions from the offset-detector data (i.e., truncated data), we also perform reconstructions from noiseless data collected over several SAs of LARs $\alpha_\tau = 150^\circ, 135^\circ, 120^\circ$ (i.e., data in row 2 of Fig. 2b-2d), and show the reconstructed images in row 2 of Fig. 3. The FDK reconstructions from the truncated TOA LAR data are shown in row 3 of Fig. 3 for demonstrating the artifacts as the combined result of LAR and data truncation issues.

It can be observed that FDK reconstructions contain significant LAR artifacts that overwhelm soft-tissue contrast of interest, and tooth structures in the reconstructed images are difficult to be discerned. DTV reconstructions from both TOA and SA data appear visually comparable to the phantom image and the LAR artifacts observed in the corresponding FDK reconstructions are significantly reduced. Although the DTV reconstructions for SA scanning configurations show clearly the tooth structures without much of the artifacts in the FDK images, there remain residual artifacts around the spine region. As the LAR α_τ is reduced from 150° to 120° , the artifacts become more significant, caused by the combination of data-truncation and LAR. Conversely, the DTV reconstructions for the TOA scanning configurations remain visually identical to the phantom image and largely free of the artifacts.

3.2 Reconstruction from noisy data

In order to investigate the robustness of the DTV reconstruction from truncated TOA and SA LAR data, we repeat the study in Sec. 3.1 with noisy data and show the results in Fig. 4. Again, for noisy LAR data considered, the DTV reconstructions for both the TOA and SA scans yield images with significantly reduced LAR artifacts as compared to the FDK reconstructions. Also, the TOA configurations appear to yield images with minimum artifacts as compared to that obtained for the SA configurations, consistent with the observation made above.

4. DISCUSSION

In this work, we have investigated accurate image reconstruction from truncated data acquired with TOA and SA scanning configurations of LARs. The investigation is enabled by tailoring the primal-dual-based DTV algorithm to reconstruct images through solving an optimization program that includes a weighted data- ℓ_2 fidelity and DTV image constraints. The study results suggest that the tailored DTV algorithm can significantly reduce the LAR artifacts that are observed otherwise in reconstructions obtained with the existing algorithms. Moreover, it is also revealed that TOA scanning configurations generally appear to be more effective than the SA scanning configurations in terms of reducing the combined LAR and data-truncation artifacts. Further investigation will focus on the impact of the extent of detector-offset, weighting matrix W , and cone-beam effect on image reconstruction from LAR data.

5. ACKNOWLEDGMENT

This work was supported in part by NIH R01 Grant Nos. EB026282 and EB023968, and NIH R21 Grant No. 1R21CA263660-01A1. The contents of this article are solely the responsibility of the authors and do not necessarily represent the official views of the National Institutes of Health.

REFERENCES

- [1] P. S. Cho, R. H. Johnson, and T. W. Griffin, "Cone-beam CT for radiotherapy applications," *Phys. Med. Biol.*, vol. 40, pp. 1863–1883, 1995.
- [2] W. Chang, S. Loncaric, G. Huang, and P. Sanpitak, "Asymmetric fan transmission CT on SPECT systems," *Phys. Med. Biol.*, vol. 40, pp. 913–928, 1995.
- [3] Z. Zhang, B. Chen, D. Xia, E. Sidky, and X. Pan, "Directional-TV algorithm for image reconstruction from limited-angular-range data," *Med. Image Anal.*, vol. 70, p. 102030, 2021.
- [4] —, "Image reconstruction from data over two orthogonal arcs of limited-angular ranges," *Med. Phys.*, p. In Press, 2022.
- [5] A. K. Louis and F. Natterer, "Mathematical problems of computerized tomography," *Proceedings of the IEEE*, vol. 71, no. 3, pp. 379–389, 1983.

- [6] A. Chambolle and T. Pock, “A first-order primal-dual algorithm for convex problems with applications to imaging,” *J. Math. Imag. Vis.*, vol. 40, pp. 1 – 26, 2011.
- [7] E. Y. Sidky, J. H. Jørgensen, and X. Pan, “Convex optimization problem prototyping for image reconstruction in computed tomography with the Chambolle–Pock algorithm,” *Phys. Med. Biol.*, vol. 57, no. 10, pp. 3065–3091, 2012.
- [8] B. Chen, Z. Zhang, D. Xia, E. Sidky, and X. Pan, “Dual-energy CT imaging with limited-angular-range data,” *Phys. Med. Biol.*, vol. 66, p. 185020, 2021.
- [9] —, “Dual-energy CT imaging over non-overlapping, orthogonal arcs of limited-angular ranges,” *J. X-Ray Sci. Technol.*, vol. 29, pp. 975–985, 2021.